

## SHOCKED AND SCORCHED: THE TAIL OF A TADPOLE IN AN INTERSTELLAR POND

R. SAHAI<sup>1</sup>, M. R. MORRIS<sup>2</sup>, M. J. CLAUSSEN<sup>3</sup>  
 raghvendra.sahai@jpl.nasa.gov  
 Draft version October 23, 2018

## ABSTRACT

We report multi-wavelength observations of the far-infrared source IRAS 20324+4057, including high-resolution optical imaging with HST, and ground-based near-infrared, millimeter-wave and radio observations. These data show an extended, limb-brightened, tadpole-shaped nebula with a bright, compact, cometary nebula located inside the tadpole head. Our molecular line observations indicate that the Tadpole is predominantly molecular, with a total gas mass exceeding  $3.7 M_{\odot}$ . Our radio continuum imaging, and archival Spitzer IRAC images, show the presence of additional tadpole-shaped objects in the vicinity of IRAS 20324+4057 that share a common E-W head-tail orientation: we propose that these structures are small, dense molecular cores that originated in the Cygnus cloud and are now being (i) photoevaporated by the ultraviolet radiation field of the Cyg OB2 No. 8 cluster located to the North-West, and (ii) shaped by ram pressure of a distant wind source or sources located to the West, blowing ablated and photoevaporated material from their heads eastwards. The ripples in the tail of the Tadpole are interpreted in terms of instabilities at the interface between the ambient wind and the dense medium of the former.

*Subject headings:* Stars: formation, Stars: pre-main sequence, Stars: protoplanetary disks, ISM: jets and outflows, ISM: individual objects: IRAS 20324+4057

## 1. INTRODUCTION

The presence of strong radiation fields from massive O and B stars can be detrimental to nearby star formation, when compared with star formation in the absence of nearby high-mass stars. Much has been published about this phenomenon; the ionizing radiation from massive stars can evaporate circumstellar disks around nearby low-mass stars (partially ionized globules, i.e. PIGS; see, e.g., Laques & Vidal 1979 and Garay 1987<sup>4</sup>) or can progressively ionize dense blobs of nearby molecular material, forming evaporating gaseous globules or EGGs, defined explicitly by Hester et al. (1996) as “globules of dense gas that are being photoevaporated more slowly than their lower density surroundings, and so are left behind as the gas around them is driven off.” These terms, which describe the ionization/evaporation of gas in disks around low-mass stars, or surrounding molecular material, are rather ill-defined otherwise. The term “proplyd” (photoevaporating protoplanetary disk) is probably the best defined, and is generally accepted as referring to evaporating circumstellar disks around young, low-mass stars. An extensive literature can be found about proplyds, especially those in the Orion Nebula Cluster (e.g. O’Dell, Wen, & Hu 1993; Ricci, Robberto, & Soderblom 2008), and their interpretation (e.g. Storzer & Hollenbach 1999; Johnstone, Hollenbach, & Bally 1998). Sizes and mass-loss rates of proplyds in the Orion Nebula Cluster range from 40–350 AU and  $0.7\text{--}1.5 \times 10^{-6} M_{\odot} \text{ yr}^{-1}$  (Henney & O’Dell 1999). The EGGs, first discovered in the Eagle Nebula, appear to be connected to ongoing star formation; near-infrared, high angular resolution observations show that  $\sim 15\%$  of

the EGGs in the “elephant trunks” of the Eagle show evidence for associated young low-mass stars, and that there is also evidence for relatively massive young stellar objects at the tips of the elephant trunks (McCaughrean & Andersen 2002). With the advent of *Spitzer* and the *Wide-field Infrared Survey Explorer (WISE)*, new imaging surveys have revealed the wide-spread presence of elephant-trunk structures (also referred to as “pillars”) and EGGs towards many massive star-forming regions (e.g., Smith et al. 2010, Koenig et al. 2012).

We have serendipitously discovered an extended, limb-brightened, tadpole-shaped nebula associated with the IRAS source IRAS 20324+4057 (I20324) near the Cygnus OB2 No. 8 cluster. This paper presents HST imaging, Palomar 5-m spectroscopy, Spitzer IRAC and MIPS imaging, VLA radio continuum imaging, and (sub) millimeter-wave spectroscopy using the ARO SMT and 12-m in order to elucidate the nature of this object and its relationship to proplyds, PIGs, or EGGs.

I20324 was observed in an HST imaging survey of a list of candidate long-lived preplanetary nebulae (PPNs) selected from the IRAS Point Source Catalog using a color-criterion ( $F_{60}/F_{25} > 1$ ) chosen to select objects that are dominated by relatively cool dust located at some distance from a stellar source, or where any hot dust is highly obscured (Sahai et al. 2007). All objects were required to have point-source 2MASS (JHK) and MSX (A band/ $8\mu\text{m}$ ) counterparts, implying the presence of local stellar sources that have heated the dust revealed in the HST and IRAS data. However, we found that a large fraction of the objects resolved in our survey reveal morphologies quite different than those found for PPNs (e.g. Sahai et al.

<sup>1</sup> Jet Propulsion Laboratory, MS 183-900, California Institute of Technology, Pasadena, CA 91109

<sup>2</sup> Department of Physics and Astronomy, UCLA, Los Angeles, CA 90095-1547

<sup>3</sup> National Radio Astronomy Observatory, 1003 Lopezville Road, Socorro, NM 87801

<sup>4</sup> Since the Garay review paper, the original PIGs have largely been recast as proplyds, and the acronym PIG has been used to describe much larger bright-rimmed molecular clouds, e.g., Serabyn, Gusten, & Mundy 1993

2007). I20324 is one of the most prominent of these. It was first detected as an emission-line nebula together with two other nebulous objects within a  $3.1' \times 3.1'$  field, in a ground-based  $H\alpha + [NII]$  survey of candidate post-AGB objects (Pereira & Miranda 2007: PM07). PM07 concluded that all 3 objects are “related young stellar objects” and that the emission-line spectrum of I20324 is indicative of photoionization rather than shock-excitation.

Independently, I20324 has been noted recently by Wright et al. (2012: Wet12), who included it among a group of 10 “proplyd-like objects” associated with the Cygnus OB2 association. They considered both the proplyd and EGG hypotheses, and concluded that neither scenario adequately explains their observations. They suggest that these and the other objects they identified are “a unique class of photoevaporating partially embedded young stellar objects”. In contrast, we find that our data favor the EGG hypothesis.

## 2. OBSERVATIONS & RESULTS

### 2.1. *HST* imaging

We obtained optical images of I20324 on 2006-07-22 using HST’s Wide-Field Camera (WFC) of the Advanced Camera for Surveys (ACS), which has a plate scale of  $0''.050/\text{pixel}$ , using the F606W ( $\lambda = 0.60 \mu\text{m}$ ,  $\Delta\lambda = 0.123 \mu\text{m}$ ) and F814W ( $\lambda = 0.80 \mu\text{m}$ ,  $\Delta\lambda = 0.149 \mu\text{m}$ ) filters. A 2-point dither was used for the imaging with a total exposure time of  $2 \times 347\text{s}$  per filter. These images show an extended nebula with a limb-brightened “tadpole” shape (hereafter, we often use the label “Tadpole” to refer to I20324) (Fig. 1a) oriented roughly E-W; the periphery of the nebula is distinctly brighter and more defined on the N side and shows prominent ripples. A bright compact knot is located interior to the tadpole head (Fig. 2). The intensity of the knot, which itself has a cometary shape, peaks at J2000  $\alpha=20:34:13.23$ ,  $\delta=41:08:14.6$  (in the F814W image), coinciding with the location of luminous point sources in the 2MASS (20341326+4108140:  $\alpha=20:34:13.26$ ,  $\delta=41:08:14.07$ ) and MSX6c catalogs (G080.1909+00.5353:  $\alpha=20:34:13.4$ ,  $\delta=41:08:14$ ). The axis of the cometary knot is aligned at a PA of  $-43^\circ$  (north through east). From the F606W image, we find that the Tadpole has a length of  $54.7''$  (76,600 AU) and a maximum width of  $14.1''$  (19750 AU). The cometary knot, seen more sensitively in the F814W image, is about  $2.4'' \times 1.3''$  (3350 AU  $\times$  1800 AU). The knot has a conical shape near the apex with an “inner” opening angle of  $55^\circ$ , but then narrows towards a more cylindrical shape at offsets greater than about  $0.75''$  implying an “outer” opening angle of  $\sim 0$ .

The cometary knot has a diametrically-opposed faint counterpart seen only in the F814W filter – the simplest interpretation of these features together is that they represent scattered light from the lobes of a collimated bipolar outflow directed along the polar axis of a flared disk (or dense equatorial region) tilted such that the near-side of the disk lies to the NW of the bright apex of the knot. Extinction by the tilted disk then explains the faintness of

the NW lobe of the bipolar outflow. The NW outflow extends toward three faint red star-like objects ( $a$ ,  $b$  and  $c$  in Fig. 2): high-resolution ( $0.15''$ ) H and  $K_s$  band images obtained with the Laser Guide Star Adaptive Optics system on the Palomar 200-in using the High-Angular Resolution Observer (PHARO) NIR camera show point sources at the locations of  $a$ ,  $b$  and  $c$  (Sahai et al. 2012, in preparation) supporting the idea that these are stars, and not simply compact disks illuminated by starlight from the Tadpole’s central star. The stars  $a$  and  $b$  show small “tail” structures emanating from them (inset: Fig 2); the inner part of star  $a$ ’s tail is roughly aligned with the bipolar outflow axis, whereas in the outer parts, the tail starts curving backwards.

I20324 falls within the region imaged by the Spitzer Cygnus X Legacy Survey program (PI: J. Hora) with the IRAC (4 bands at 3.6, 4.5, 5.8, and  $8.0 \mu\text{m}$ ) and MIPS instruments (2 bands at 24 and  $70 \mu\text{m}$ ) – since some of these data have been recently reported by Wet12, we do not discuss them in detail. Inspection of the Legacy Cygnus-X Spitzer images reveals a bright point-source in all four IRAC bands and the MIPS 24  $\mu\text{m}$  band, together with a tail structure. The coordinates of the point source in the Cygnus-X catalog are RA=20:34:13.23, Dec=41:08:14.1, virtually identical with the location of the cometary knot apex in the HST images. The 8  $\mu\text{m}$  image is notable in showing the ripples on the South periphery of the Tadpole (Fig. 1b), which are also seen in the HST image but less clearly. Although the angular resolution is rather limited relative to the object’s size at 70  $\mu\text{m}$ , the MIPS image shows a cometary shape with a bright head which is likely dominated by flux from the central source in the Tadpole. We assume that I20324 is associated with the Cygnus OB2 association, and adopt a distance,  $D = 1.4\text{kpc}$  (Rygl et al. 2012)<sup>5</sup>.

### 2.2. Additional Multi-wavelength Observations

Following the HST observations, we obtained supporting ground-based observations with (i) the Palomar 5-m (ii) the Very Large Array (VLA) of the NRAO<sup>6</sup>, and (iii) the 10-m (SMT, Mt. Graham, AZ) and 12-m (Kitt Peak, AZ) (sub)millimeter-wave telescopes of the Arizona Radio Observatory (ARO).

The TripleSpec Spectrograph at Palomar was used to observe I20324 with its  $1'' \times 30''$  slit aligned N-S, so as to cut laterally across the Tadpole body, at two locations (i) passing through the cometary knot (Slit 1), and (ii)  $12''$  E of the knot (Slit 2). The seeing was about  $1''$  at K-band. Strong emission from  $H_2$  S(1),  $v=1-0$  and other  $H_2$  lines was detected in both slits; for Slit 2, the emission is clearly limb-brightened (Fig. 1b). The Slit 1 spectra also show a strong continuum at the position of the cometary knot, and extended emission in the HI  $Br\gamma$  and  $Pa\beta$  lines – the latter lines display a local peak centered on the knot.

The VLA was used in the C configuration to observe the field near the Tadpole nebula in August 2009, as part of program AS980. Observations were made at frequencies 8.5 and 22.5 GHz ( $\lambda=3.6$  and 1.3 cm, respectively).

<sup>5</sup> Previous distance estimates to Cyg OB2 have been generally higher, with  $D \sim 1.7\text{kpc}$  (Hanson 2003); derived values of masses and luminosity in this paper scale as  $D^2$ .

<sup>6</sup> the National Radio Astronomy Observatory is a facility of the National Science Foundation operated under cooperative agreement by Associated Universities, Inc.

Standard data editing, calibration, imaging, and deconvolution were performed using the Astronomical Imaging Processing System (AIPS) for both frequencies. For the 8.5 GHz image, observed on 05 August (Fig. 3), the restoring beam was  $3.2'' \times 2.8''$  at  $PA = -65^\circ$ . The rms noise in the final image was  $\sim 65 \mu\text{Jy beam}^{-1}$ . For the 22.5 GHz image (observed on 10 August), a  $70 k\lambda$  taper was applied in the imaging step to provide a similar angular resolution to the 8.5 GHz image. The VLA 8.5 GHz image shows a tadpole-shaped structure at the location of I 20324 and two additional sources, which were also detected in the PM07 emission-line survey (objects B & C in their Fig. 1; object A is I 20324). IRAC  $8 \mu\text{m}$  images (insets in Fig. 3) of objects B & C show similarly elongated morphologies: given its resemblance to a goldfish, we dub object B, the “Goldfish”. We also searched for the water maser emission line at 22.235 GHz towards the Tadpole, but did not detect any emission over a total  $V_{lsr}$  range of  $\pm 41.85 \text{ km s}^{-1}$  to a  $1\sigma$  sensitivity of  $25 \text{ mJy beam}^{-1}$  per  $48.83 \text{ kHz}$  wide channel.

The total flux densities at 8.5 GHz for the Tadpole, Goldfish and object C are  $55 \pm 1.2$ ,  $10 \pm 0.4$ , and  $6 \pm 0.7 \text{ mJy}$ . At 22.5 GHz, only the Tadpole is detected with a flux density of  $30 \pm 1.4 \text{ mJy}$ . The significantly lower flux density at 22.5 GHz compared to that at 8.5 GHz for the Tadpole implies the presence of non-thermal emission in this source. The radio emission peaks strongly along the shock/ionization front at the head of the Tadpole, possibly as a result of a compressed magnetic layer in this front that is interacting with cosmic rays (CRs) associated with the Cyg OB2 association – we note that the Fermi Large Area Telescope has recently revealed a 50-parsec wide cocoon of freshly accelerated CRs that fill the cavities carved in the Cygnus star-forming region by stellar winds and ionization fronts (Ackermann et al. 2011). Further observations at different radio wavelengths are needed to confirm and explore the nature of non-thermal emission from the Tadpole.

We estimate a total mass of ionized gas in the Tadpole of  $\lesssim 10^{-2} M_\odot$ , assuming optically-thin free-free emission at 22.5 GHz, and approximating the emitting region with a triangular slab (of area  $375 \text{ arcsec}^2$ ), which fits the Tadpole’s projected shape in the 8.5 GHz image. Our mass estimate is an upper limit since there may be a non-thermal contribution at 22.5 GHz.

The ARO data were taken during 2009 Jan-May. The  $^{12}\text{CO}$ ,  $^{13}\text{CO}$  J=2–1 lines and the  $\text{HCO}^+$  J=3–2 line were observed with the 1 mm dual-polarization receiver employing ALMA Band 6 SBS mixers on the SMT 10-m, and filterbanks with 1 MHz resolution. Typical system temperatures were 240 K (770 K) for the CO ( $\text{HCO}^+$ ) observations. The beam size was  $\theta_b = 32''$  at 1.3 mm, and pointing accuracy was estimated to be about  $\pm 4''$ . The  $^{12}\text{CO}$  and CS J=2–1 lines were observed with the 12-m telescope at Kitt Peak using dual-polarization SIS receivers. Typical system temperatures were 430 K (240 K) for the CO (CS) observations, and data were recorded with the Millimeter Autocorrelator (MAC) configured to provide 48.8 kHz resolution. The beam size was  $\theta_b = 60''$  at 2.6 mm, and pointing accuracy was estimated to be about  $\pm 6''$ . Observations were conducted in position-switching mode using an off position  $15'$  South of I 20324 which was tested to be

free of significant emission.

The spectra of the high-density tracer lines,  $\text{HCO}^+$  J=3–2 and CS J=2–1 (Fig. 4), show strong emission peaking at  $V_{lsr} = 10.4 \text{ km s}^{-1}$ , indicating that the peak density in the emitting region is quite high<sup>7</sup>,  $\sim 10^6 \text{ cm}^{-3}$ . The map ( $5' \times 5'$ ) of the CO and  $^{13}\text{CO}$  J=2–1 emission (with both lines being observed simultaneously) using the “on-the-fly” mapping technique shows a compact source peaking at the same  $V_{lsr}$  (Fig. 5) centered on the Tadpole (object A). A second nearby peak coincides with the Goldfish. The CO emission from I 20324 is extended along the E-W direction with a FWHM of about  $45''$  and it is unresolved in the N-S direction; source B is unresolved. Sparse mapping of the  $\text{HCO}^+$  J=3–2 emission shows that it is also extended E-W. There is also extended, structured emission in the velocity range  $V_{lsr} = -5$  to  $8 \text{ km s}^{-1}$  that is not connected spatially or kinematically with the Tadpole or Goldfish, but likely comes from the same complex of progenitor molecular clouds that spawned them.

We derive an excitation temperature,  $T_{ex} = 11 \text{ K}$  from the peak intensity ( $T_R = 6.2 \text{ K}$ ) of the CO J=2–1 line, assuming it to be optically thick. Assuming LTE conditions, we find (using the RATRAN online code: Van der Tak et al. 2007), that the peak  $^{13}\text{CO}$  J=2–1 line intensity ( $T_R = 2.5 \text{ K}$ ) and observed line-width ( $2 \text{ km s}^{-1}$ ), imply a total column density  $N(\text{H}_2) = 0.4 \times 10^{22} \text{ cm}^{-2}$ , assuming a standard interstellar  $^{13}\text{CO}/\text{H}_2$  abundance ratio of  $10^{-6}$  (e.g., Hayashi et al. 1993). This gives a total molecular mass of  $3.7 M_\odot$  for I 20324. Assuming a similar kinetic temperature and abundance for Source B, we find its mass is about  $1.3 M_\odot$  (its peak  $^{13}\text{CO}$  J=2–1 line intensity is about half that of I 20324). Our mass estimates are likely lower limits because the “standard” value adopted for the  $^{13}\text{CO}/\text{H}_2$  abundance ratio may be too large since a significant fraction of CO (and  $^{13}\text{CO}$ ) may have been photodissociated in a PDR that occupies much of the volume of the tadpoles.

### 3. THE NATURE OF I 20324

The Tadpole is detected at all wavelengths from the near- to the far-infrared, with point-source counterparts in the 2MASS, MSX, IRAS, and Akari catalogs: the spectral energy distribution (SED) is shown in Fig. 6. We have also included the IRAS Low Resolution Spectrum (LRS) spectrum for the Tadpole (with a correction of the absolute calibration applied as described by Cohen, Walker, and Wittborn (1992)). Since the LRS data were rather noisy, we increased the S/N ratio by binning the spectrum to a factor 3 lower resolution: a weak  $10 \mu\text{m}$  silicate dust feature can be seen in absorption. The IRAC photometry was extracted from Cygnus-X catalog, whereas the MIPS photometry was derived from the Legacy Cygnus-X images using aperture photometry. The core of the  $24 \mu\text{m}$  image of I 20324 is partly saturated, so we used the bright Airy ring at a radius of  $26.5''$  from the center (4th ring) for measuring the flux; our estimate of 37 Jy is consistent with the IRAS flux value. Comparing the Spitzer photometry with that from missions having lower angular resolution (red symbols) at similar wavelengths (24 and  $70 \mu\text{m}$ ), we find that the former (hereafter the “small aperture” fluxes) fall systematically below the latter at  $\lambda \sim 60 - 70 \mu\text{m}$ .

<sup>7</sup> The critical density for collisional excitation of the  $\text{HCO}^+$  J=3–2 line is  $> 3.9 \times 10^6 \text{ cm}^{-3}$  in a cloud at a temperature of  $< 20 \text{ K}$

This indicates the presence of an extended source of warm dust at these wavelengths heated by the external radiation field, in addition to the compact central source, which looks point-like out to a wavelength of at least  $24\ \mu\text{m}$ . The large mid- and far-IR fluxes of this point-source imply the presence of a substantial mass of circumstellar dust around the Tadpole’s central star. The total source luminosity of the Tadpole derived from integrating the “small aperture” SED is about  $500L_{\odot}$ , implying that the Tadpole’s central star is not a low-mass star. From an inspection of pre-main-sequence stellar evolutionary tracks by Bernasconi & Maeder (1996), we find that our estimated luminosity implies a stellar mass of around  $5M_{\odot}$  if the star has just begun deuterium burning, or somewhat lower if it is approaching the main-sequence.

We fitted I20324’s “small aperture” SED using the on-line tool provided by Robitaille et al. (2007), which computes least-squares fits of pre-computed models of young stellar objects (YSOs) having disks and rotationally-flattened infall envelopes (with biconical outflow cavities), to user-defined SEDs. We set the input distance range to  $D=1.3\text{--}1.6\text{ kpc}$ . The input interstellar extinction range was set to  $A_v = 0 - 2$ , based on our estimate of  $A_v = 0.7 \pm 0.7$  using the numerical algorithm provided by Hakkila et al. (1997), which computes the 3-dimensional visual interstellar extinction and its error from inputs of Galactic longitude, latitude, and distance, from a synthesis of several published studies. The best-fit model has  $D=1.4\text{ kpc}$ ,  $A_v = 1.5$ , and a central star mass,  $M_* = 4.6 M_{\odot}$  and effective temperature,  $T_{eff} = 4140\text{ K}$ ; the model spectrum shows the presence of a weak silicate absorption feature as observed (Fig. 6). In this model, the full opening angle of the bipolar outflow cavity is  $\theta_c = 7^{\circ}$ , and the outflow cavity axis is inclined at a modest angle of  $i = 18^{\circ}$ , to the line-of-sight. The next best model has  $D=1.4\text{ kpc}$ ,  $A_v = 2$ ,  $M_* = 6.5 M_{\odot}$ ,  $T_{eff} = 4200\text{ K}$ ,  $\theta_c = 5^{\circ}$ , and  $i = 18^{\circ}$ , however the depth of the silicate feature relative to the continuum, is twice that observed. In both models, almost all of the emitting mass is associated with the envelope. These models are qualitatively consistent with the optical appearance of the luminous central source, with scattered light from the inner regions of the near-side bipolar cavity producing the cometary knot seen in the HST image, and its farside counterpart being obscured by the dense inner equatorial region of the envelope. The value of the de-projected opening angle in the best-fit model,  $i_{corr} = \tan^{-1}(\tan \theta_c / \sin i) = 23^{\circ}$ , lies in the range covered by the inner and outer opening angles of the knot ( $0 - 55^{\circ}$ ). We note that the minimum inclination angle in the model is  $i = 18^{\circ}$ , so it is possible that a better fit might have been obtained with a smaller inclination angle which would result in a larger value of  $i_{corr}$ . However, a better  $10\ \mu\text{m}$  spectrum covering the silicate feature (i.e., with higher S/N and a small aperture) is needed before the derived parameters from the above modelling can be put on a firm footing.

We note that there are several tadpole-shaped objects in the vicinity of I20324 that share with the latter a common E-W head-tail orientation. These are: (i) the Goldfish (outside the field-of-view in our HST images; #8 in Wetall2), (ii) “object C” of PM07 seen faintly in the 8.5 GHz, HST and Spitzer images, which has a relatively small tail

(#9 in Wetall2), (iii) and an object at RA=20:34:45.9, Dec=41:14:46.5 in the IRAC images of this region (#10 in Wetall2). The common E-W orientation strongly suggests these structures are shaped by the ram pressure of a passing wind from a distant source or sources located to the West of these objects, with material being ablated from their heads and blown eastwards. Noting that the tails in both the Tadpole and Goldfish are bright on their northern sides (both in the optical and in the radio), we conclude that this is due to asymmetric irradiation of these objects by the ultraviolet radiation field of the Cyg OB2 No. 8 cluster that lies to NW of the Tadpole and Goldfish, at a separation of about  $900''$  ( $\sim 6\text{ pc}$ ).

The Tadpole and its associates are most likely small, dense molecular cores near the Cyg OB2 complex that are being subjected to photoevaporation by the strong UV radiation field due to the large number of O stars in this massive star formation region. The presence of additional young stars (objects *a*, *b*, and *c*: Sahai et al. 2012, in preparation) in close physical proximity to I20324’s cometary knot indicates that several young stars have formed within the dense molecular core inside the head of the Tadpole. The small tails associated with *a* and *b* may represent (i) winds from these stars interacting with the NW outflow of, or (ii) possibly photoevaporation of their circumstellar disks by radiation from, the Tadpole’s central star. The curvature of *a*’s tail away from the Tadpole’s head may be due to interaction with the compressed “wall” of gas in the latter (note that the wall curves around both the back and the front, so *a* could be located quite close to the rear Tadpole wall).

The physical processes responsible for producing the radio-bright peripheries of the Tadpole and its associates are likely the same ones that operate in the vicinity of the M16 (Eagle Nebula) elephant trunks (lateral width  $\sim (0.5 - 1) \times 10^{18}\text{ cm}$ ) where dense, dusty molecular clouds are being eroded by photoevaporation due to radiation from O stars at a distance of  $6 \times 10^{18}\text{ cm}$  from the trunks, producing a photoevaporative flow. The heads of these trunks appear in emission-line images as limb-brightened arcs at the interface between the molecular cloud and the ambient HII region. The bright heads (size  $\sim 3 \times 10^{17}\text{ cm}$ ) and bodies of the Tadpole and its associates likely represent similar interfaces.

We interpret the ripples evident in the Tadpole body as resulting from Kelvin-Helmholtz (K-H) instabilities. Such instabilities are expected to occur at the periphery of a dense cloud embedded in diffuse gas, when there is relative motion between the two components (e.g., Fleck 1984, Kamaya 1998). The spatial wavelength of the ripples ( $\sim 15'' = 3.2 \times 10^{17}\text{ cm}$ ) is very similar to the wavelengths of the “ripples” found on the surfaces of some molecular clouds in the Orion nebula by Berné et al. (2010) that have also been interpreted as resulting from K-H instabilities. We consider (but discard) the possibility that the ripples could be caused by the orbital motion of two bound stars separated by a distance comparable to the ripple amplitude ( $\gtrsim 2'' = 2800\text{ AU}$ ), since the ripple wavelength implies a time scale of  $1050\text{ yr}$  ( $100\text{ km s}^{-1}/V_w$ ) ( $V_w$  is an assumed speed for the exterior wind impacting the Tadpole), which is much shorter than the expected orbital time for such a binary system,  $10^5\text{ yr} (M_1 + M_2)^{-1/2}$  (taking the masses

of the stars in the binary to be  $M_1 \sim M_2 \sim 1 M_\odot$ ).

Although the bow-shock morphology of the head of the tadpole structure and the cometary shape of the central knot in I20324 are very similar to the shapes of structures seen towards proplyds in the Orion star-forming region (e.g., O’Dell & Wong 1996, Bally et al. 1998), we do not think I20324 or object B are proplyds because the associated molecular masses (greater than 3.7 and 1.3  $M_\odot$ ) are much too large compared to what one might expect for circumstellar material being evaporated from protoplanetary disks: disk masses of (0.003–0.07)  $M_\odot$  have been inferred from an SMA continuum survey for the Orion proplyds (Mann & Williams 2010). Indeed, no dense molecular medium has yet been found around the central disks in any known proplyd. Furthermore, the minimum separation between the bright periphery of the Tadpole head (which would represent the wind shock in the proplyd hypothesis) and the cometary knot in I20324 is  $4.7'' = 6600$  AU, is much larger than the corresponding typical separations for the Orion proplyds ( $\sim 500 - 1000$  AU: Bally et al. 1998). However, this argument needs to be strengthened by a quantitative assessment of the competing effects of (i) the larger number of ionizing stars in Cyg OB2 and, (ii) their larger distance from the location of I20324 and its associates compared to Orion, since the physical scales of structures associated with proplyds scale inversely with the ionizing EUV flux.

We conclude that I20324 and its associates are EGGs. EGGs are likely to be the surviving dense portions of their parent molecular clouds, and as such, they should be predominantly molecular, as observed in our objects. While the original concept of EGGs shows them as having elongated tails that connect them continuously with the elephant trunks in M16, this is due to the ionizing sources in M16 being concentrated in one direction relative to the EGGs. However, the presence of multiple ionizing sources distributed over a large solid angle relative to the EGGs, as in Cyg OB2, results in a diffuse radiation field that eventually pinches off their tails – a possibility noted by Hester et al. (1996), and supported by numerical simulations (e.g., Ercolano & Gritschneider 2011) – creating “free-floating” EGGs, such as the Tadpole and its associates.

Their relatively high internal density has not only prolonged their survival in the hostile radiative and windy environment of the Cyg OB2 cluster, but it makes these globules a likely place for stars to have begun forming, especially as the overpressure of the surrounding HII region would have aided gravity by compressing the globules. It therefore seems to be no accident that the Tadpole and the Goldfish have embedded stars. Wetal12 point out that a higher fraction of the globules in this region (70%) appear to have stars than those in the Eagle Nebula (15%), and they use this fact to argue that their objects in Cygnus are therefore unlikely to be EGGs. However, several variables can affect this fraction. The parent cloud of the Eagle Nebula may have been considerably less dense and massive than the parent cloud of the globules in Cygnus, and the Cygnus OB2 association could provide a much stronger radiation field and more powerful winds than the cluster powering the Eagle Nebula. Both of these factors would affect both the size distribution of the resulting EGGs and the compression to which they are subjected.

In summary, it is quite plausible that not only the Tadpole and the Goldfish, but all of the “proplyd-like” objects listed in Wetal12 are EGGs, considering their rather similar physical sizes and shapes. Molecular-line observations of these objects, like the ones reported in this paper, will help in determining their masses and thus confirming their true nature.

#### 4. ACKNOWLEDGMENTS

We thank Anna Rosen for her valuable help in reducing the ARO on-the-fly data presented in this paper, as part of her Spring 2009 NASA/USRP student internship at JPL. We thank the staff of the Arizona Radio Observatory for granting us observing time. The National Radio Astronomy Observatory is a facility of the National Science Foundation operated under cooperative agreement by Associated Universities, Inc. RS’s contribution to the research described here was carried out at the Jet Propulsion Laboratory, California Institute of Technology, under a contract with NASA. Financial support was provided by NASA through a Long Term Space Astrophysics award to RS and MM, and HST GO award 10536 to RS.

#### REFERENCES

- Ackermann, M., Ajello, M., Allafort, A., et al. 2011, *Science*, 334, 1103  
 Bally, J., Sutherland, R.S., Devine, D. and Johnstone, D. 1998, *AJ*, 116, 293  
 Bernasconi, P. A., & Maeder, A. 1996, *A&A*, 307, 829  
 Berné, O., Marcelino, N., & Cernicharo, J. 2010, *Nature*, 466, 947  
 Ercolano, B., & Gritschneider, M. 2011, *MNRAS*, 413, 401  
 Fleck, R.C. 1984, *AJ*, 89, 506  
 Garay, G. 1987, *Rev. Mexicana Astron. Astrop.*, 14, 489  
 Hanson, M.M. 2003, *ApJ*, 597, 957  
 Hayashi, M., Ohashi, N., & Miyama, S. M. 1993, *ApJ*, 418, L71  
 Hakkila, J., Myers, J.M., Stidham, B.J. & Hartmann, D.H. 1997, *AJ*, 114, 2043  
 Henney, W. J. & O’Dell, C. R. 1999, *AJ*, 118, 2350  
 Hester, J. J. et al. 1996, *AJ*, 111, 2349  
 Johnstone, D. Hollenbach, D. & Bally, J. 1998, *ApJ*, 499, 758  
 Kamaya, H. 1998, *ApJ*, 506, 289  
 Koenig, X. P., Leisawitz, D. T., Benford, D. J., et al. 2012, *ApJ*, 744, 130  
 Laques, P. & Vidal, J. L. 1979, *A&A*, 73, 97  
 Mann, R. K. & Williams, J. P. 2010 *ApJ*, 725, 430  
 McCaughrean, M. J. & Andersen, M. 2002, *A&A*, 389, 513  
 O’Dell, C. R., Wen, Z. & Hu, X. 1993, *ApJ*, 410, 696  
 O’Dell, C. R. & Wong, K. 1996, *AJ*, 111, 846  
 Pereira, C.B. & Miranda, L.F. 2007, *A&A*, 231  
 Ricci, L., Robberto, M. & Soderblom, D. R. 2008, *AJ*, 136, 2136  
 Robitaille, T. P., Whitney, B. A., Indebetouw, R., & Wood, K. 2007, *ApJS*, 169, 328  
 Rygl, K. L. J., 2012, *A&A* (in press, arXiv 1111.7032v2)  
 Sahai, R., Morris, M., Sánchez Contreras, C., & Claussen, M. AJ, 2007, 134, 2200  
 Serabyn, E., Guesten, R., & Mundy, L. 1993, *ApJ*, 404, 247  
 Smith, N., Povich, M. S., Whitney, B. A., et al. 2010, *MNRAS*, 406, 952  
 Störzer, H. & Hollenbach, D. 1999, *ApJ*, 515, 669  
 Van der Tak, F.F.S., Black, J.H., Schier, F.L., Jansen, D.J., van Dishoeck, E.F., 2007, *A&A* 468, 627  
 Wright, N. J., et al. 2012, *ApJ*, 746, L21

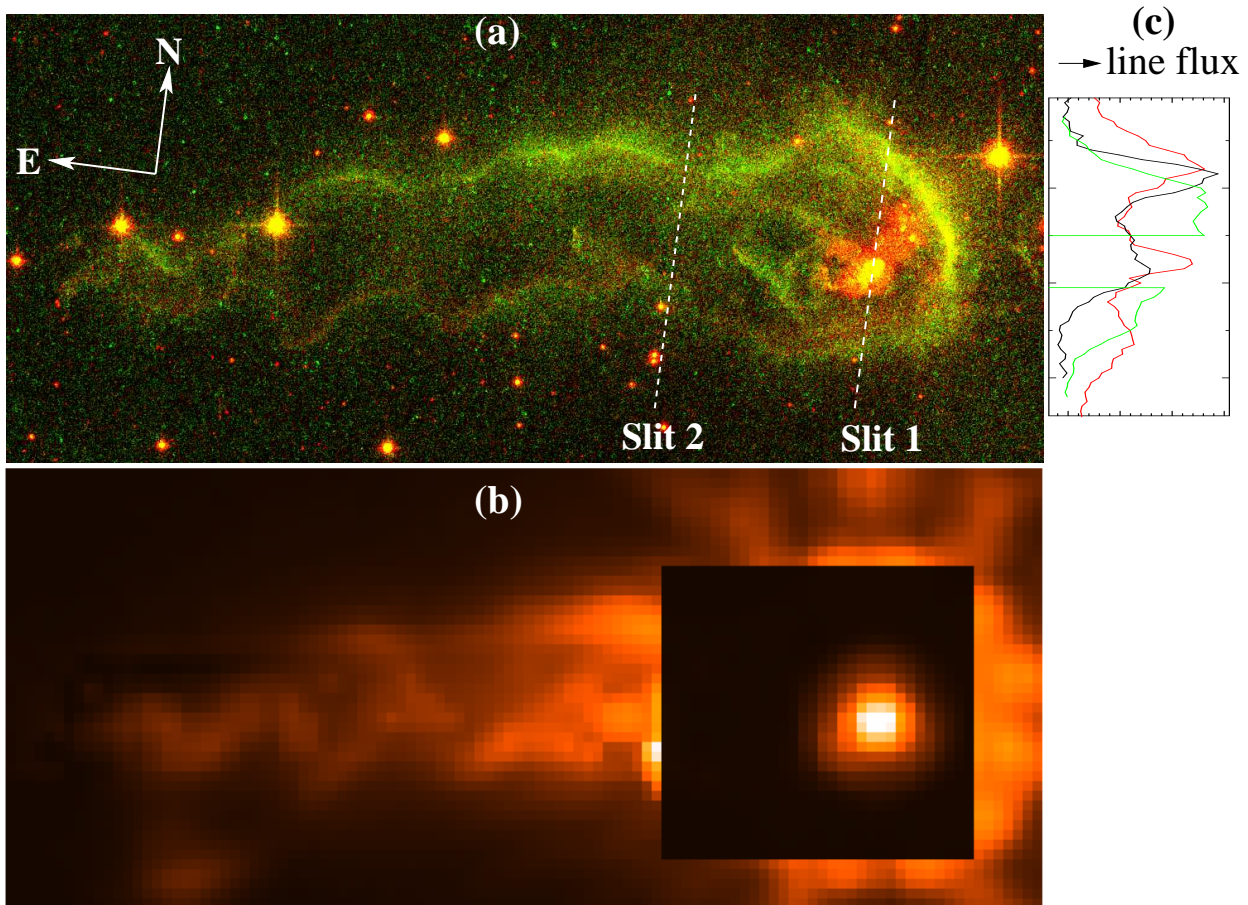


FIG. 1.— (a) Composite HST ACS/WFC (false-color) image (size  $62.7'' \times 27.1''$ ) of I20324 taken through two broad-band filters F606W (*green*) and F814W (*red*). (b) False-color IRAC  $8 \mu\text{m}$  image of same field-of-view as in panel *a*: the intensity in a  $19.2'' \times 18''$  box centered on the central star of I20324 has been scaled by a factor 0.01 in order to clearly show the much fainter tail structure. Linear stretches have been used for the images in these panels. (c) Spatial intensity cuts of near-infrared emission lines as seen through a  $1''$  wide slit, at two locations towards I20324 – Slit 1: (*green*)  $2.1 \mu\text{m}$  H<sub>2</sub>  $v=1-0$ , S(1) & (*red*)  $1.28 \mu\text{m}$  Pa  $\beta$ ; Slit 2: (*black*) H<sub>2</sub>  $v=1-0$ , S(1). The continuum emission from the

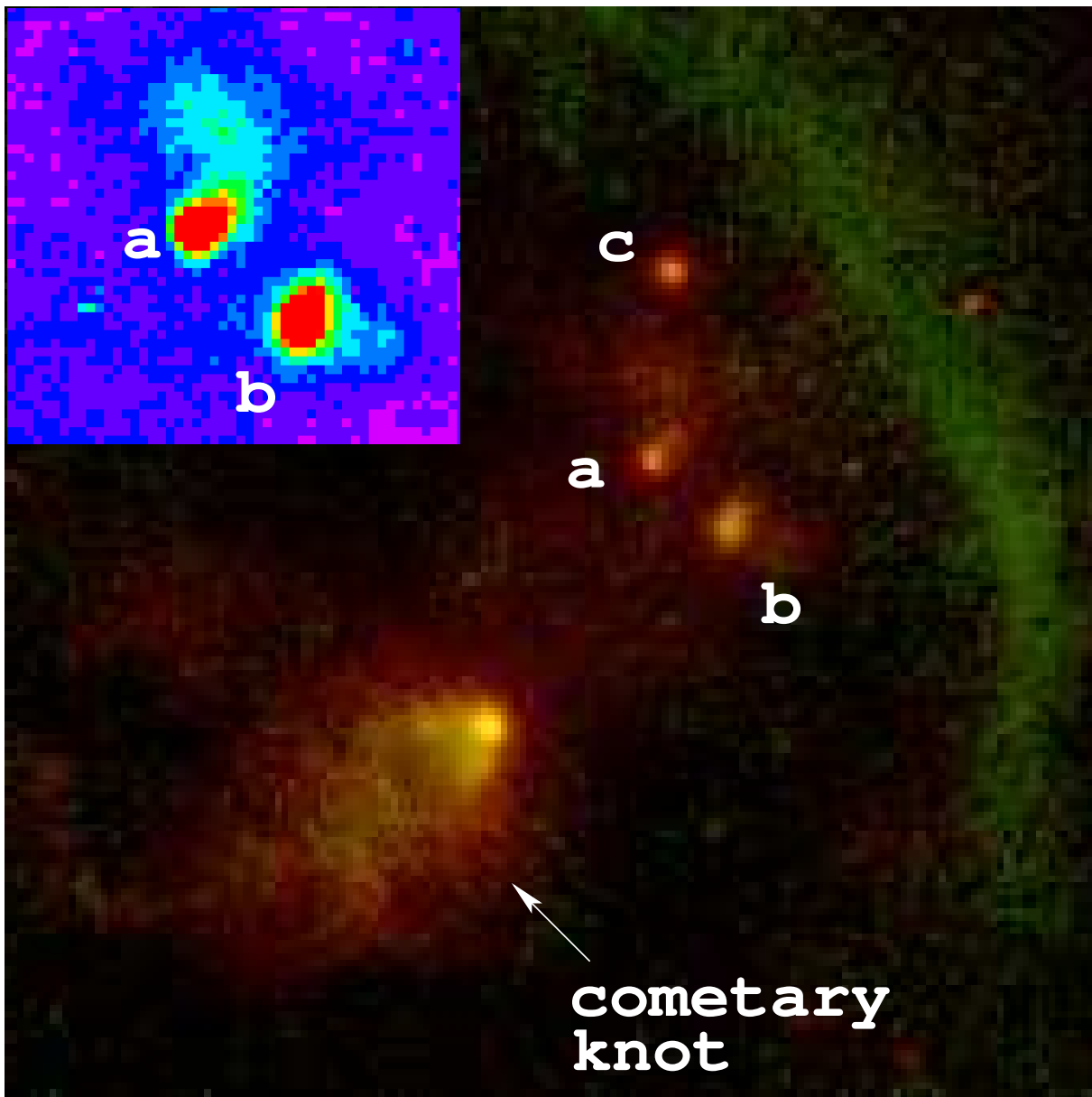


FIG. 2.— As in Fig. 1(a), but for a  $8.5'' \times 8.5''$  region covering the cometary knot (a logarithmic stretch has been used to display each of the F606W and F814W images in the color composite). Inset shows the F814W image of the region around stars *a* and *b* in false-color to emphasize the faint tail structures.

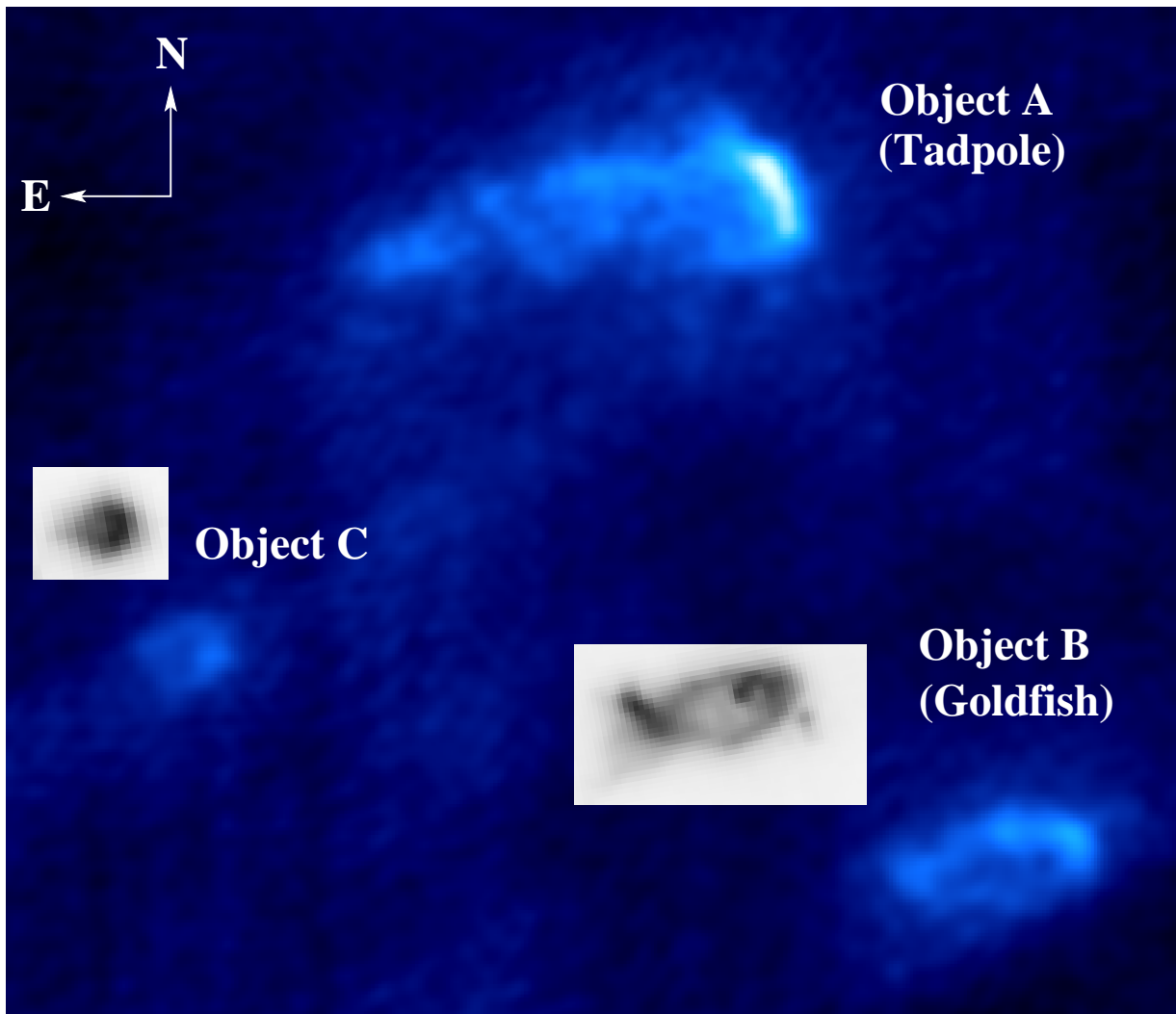


FIG. 3.— VLA map of the radio emission at 8.5 GHz from I 20324. Panel size is  $137.7'' \times 111.6''$ . The beam is  $3.2'' \times 2.8''$  and the rms noise is  $\sim 65 \mu\text{Jy beam}^{-1}$ . The peak radio intensities towards the Tadpole, Goldfish and Object C are 1.33, 0.90, and  $0.57 \text{ mJy beam}^{-1}$ . Insets show IRAC  $8 \mu\text{m}$  images of objects B and C, on the same angular scale.



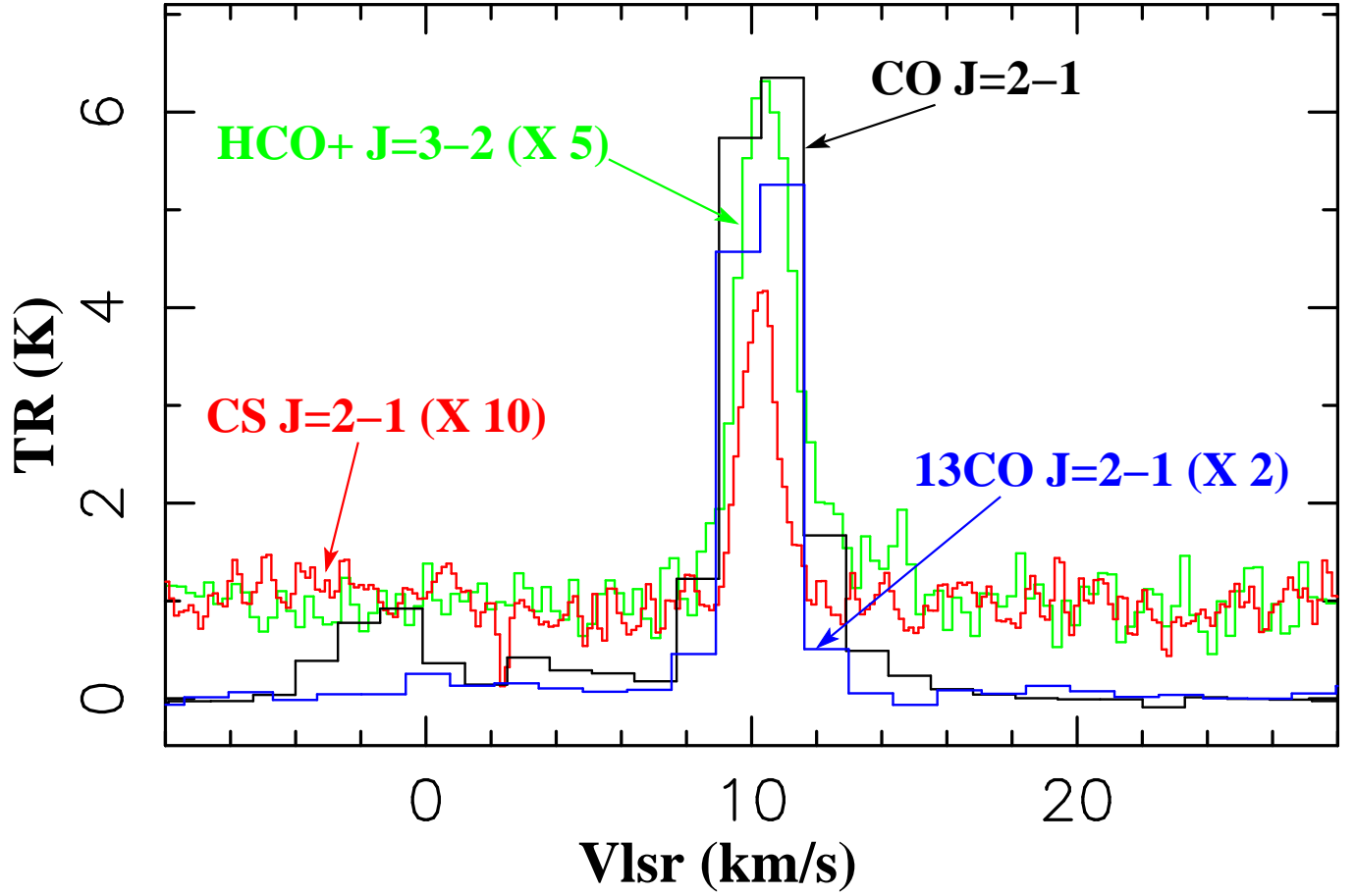


FIG. 4.— Molecular line emission from I 20324, observed with the ARO's 12-m and 10-m telescopes. For clarity, the  $^{13}\text{CO}$  J=2-1, CS J=2-1 and  $\text{HCO}^+$  J=3-2 lines have been rescaled; the rescaled CS and  $\text{HCO}^+$  lines have been shifted vertically by 1 K. The weak CO emission centered at  $V_{lsr} \sim -2 \text{ km s}^{-1}$  is due to emission from an extended molecular cloud (see Fig. 5).

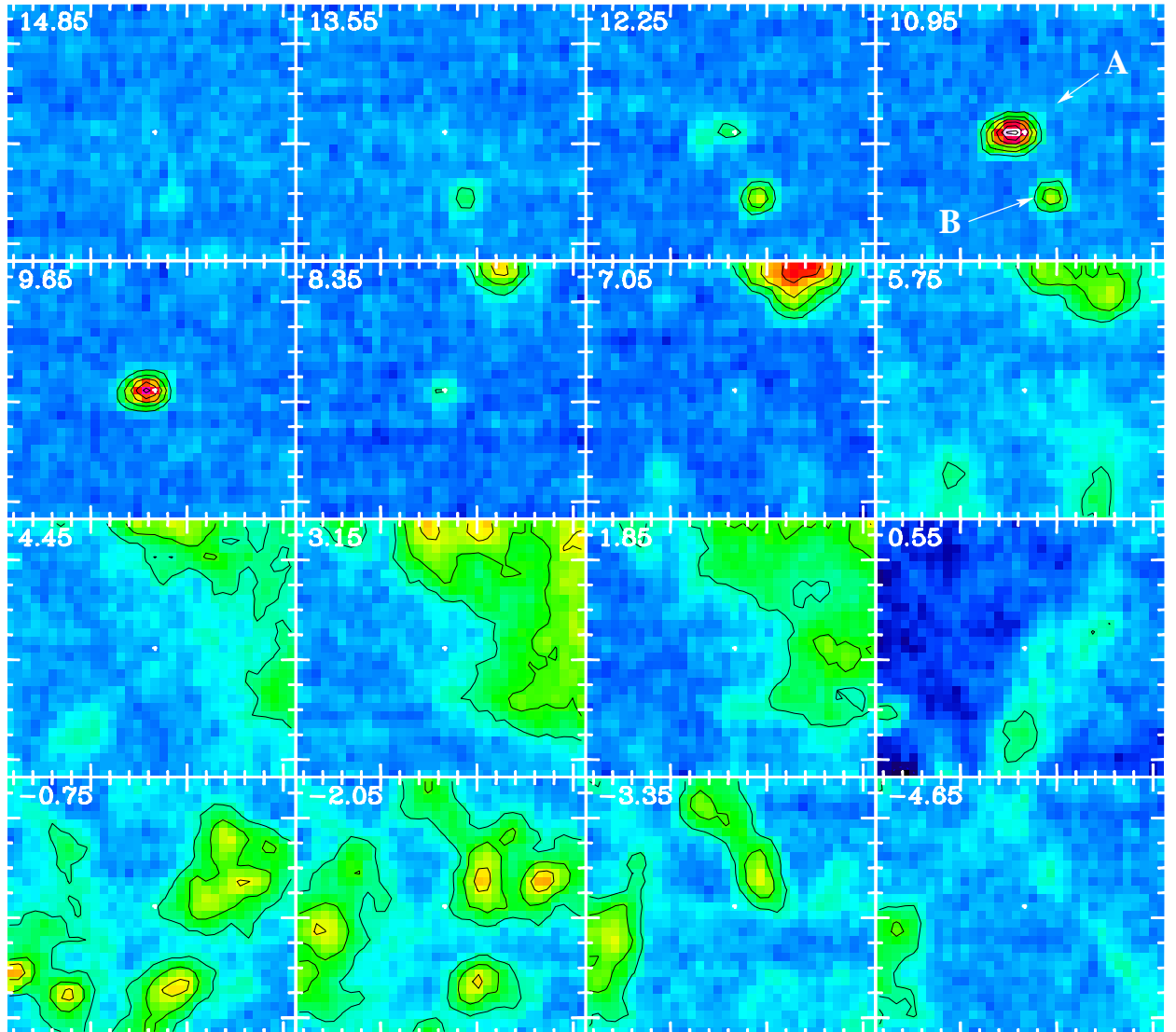


FIG. 5.— Map of the CO J=2–1 emission towards I 20324, obtained with the ARO 10-m, with each panel showing the average emission over a  $1.3 \text{ km s}^{-1}$  wide channel, centered at the LSR velocity shown in the top left corner. The small tickmarks on the x- and y-axes are spaced by  $0.5'$  and the contours are at 1, 2, 3, 4, 5, & 6 K. The CO emission clumps associated with the Tadpole (“A”) and the Goldfish (“B”) are labelled.

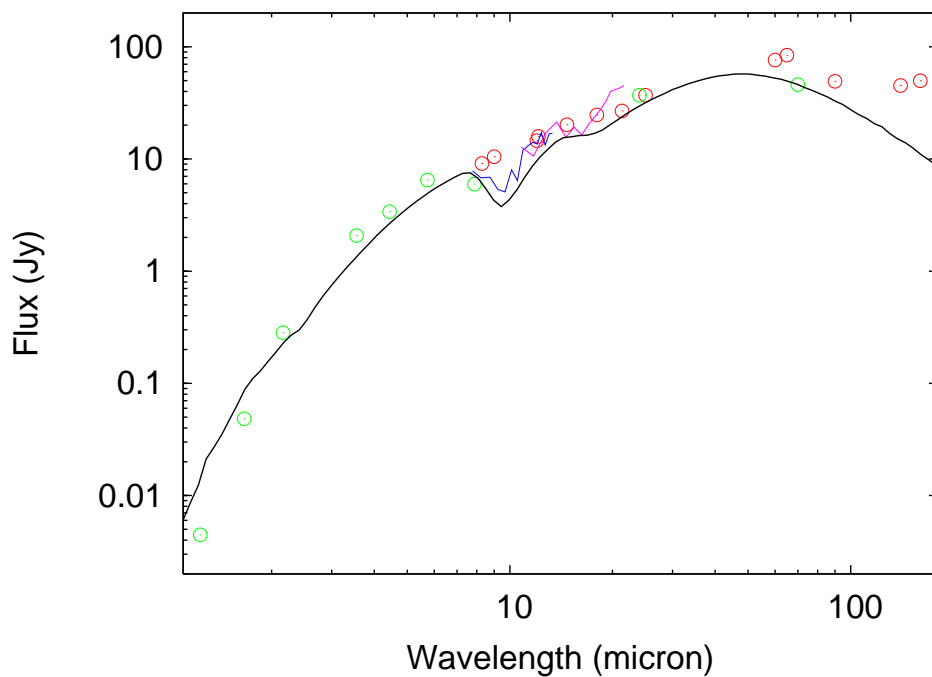


FIG. 6.— The spectral energy distribution of I20324. The red circles show photometry from MSX, IRAS, and Akari, and the green circles show photometry from 2MASS and Spitzer – the systematic errors in the photometry (not shown) are smaller than the symbol sizes (which correspond to  $\pm 15\%$  errors). Blue and magenta curves show the IRAS/LRS short-wavelength (SW: 7.7–13.4  $\mu\text{m}$ ) and long-wavelength (LW: 11–22.6  $\mu\text{m}$ ) spectrum. The black curve is the SED of a pre-computed disk-envelope model for a young stellar object with a central star of mass  $4.6M_{\odot}$ .